PHYSICS

Topological robustness of optical skyrmions through a real-world free-space link

Cade Peters[1], Vagharshak Hakobyan[2], Alice Drozdov[3], Etienne Brasselet[2], Mitchell Cox[3], Andrew Forbes[1]*

Structured light offers a promising solution for the increasing data demands of modern optical networks, opening up degrees of freedom that can be leveraged for greater channel capacity and more bits per photon. However, its implementation is hindered by real-world distortions, for example, atmospheric turbulence in free space, with severe and rapidly evolving phase perturbations that alter the amplitude, phase, and vectorial polarization structure of the beam. Here, we demonstrate that optical topologies in the form of skyrmions are highly resilient to the effects of real-world atmospheric turbulence. We create and transmit these particle-like topologies of light through a 270-meter free-space optical link, revealing their robustness across a wide variety of conditions and turbulence strengths. While we observe severe distortion in the states' underlying degrees of freedom, we show that the topological numbers are preserved in all cases. We account for fast changes to the medium, where the channel produces statistically averaged outcomes, by probing the state's decoherence, showing that while the degree of polarization consequently decays, the topology remains intact. Using topology, we show that information can be transmitted through the channel with almost perfect fidelity (>98%) in most cases, only decreasing to 86% in the most severe conditions tested. This work idemonstrates the potential for optical topologies as reliable and robust information carriers in a real-world environment and points to the potential for other complex channels too, offering attractive features for classical and quantum communication alike.

INTRODUCTION

The use of light to transmit information has had a profound impact on how we communicate. The ever increasing need for higher transmission speeds and greater bandwidths has driven a wide variety of research efforts, with l encoding schemes that involve multiplexing in time (*1*), wavelength (*2*), polarization (*3*), and combinations of these (*4*, *5*), allowing for advances in modern communication networks. Free-space optical communications (FSOC) has especially attracted interest, with the ability to establish high-speed, secure, and license-free communication links that are energy efficient and easy to deploy (*6*, *7*). Structured light (*8*) offers the potential to further increase the capacity of these channels through the use of space-division (*9*–*11*) and mode-division multiplexing (*12*–*14*) enabled by the tailoring of multiple degrees of freedom (DoFs) in both classical and quantum regimes (*15*–*17*).

The primary factors limiting the use of structured light in these contexts are the deleterious effects of the complex phase profiles and optical scatterers present in the real-world media through which light propagates. This includes biological tissue (*18*–*20*), optical fiber (*21*), and, for FSOC, atmospheric turbulence (*22*). Nonuniform refractive index profiles caused by variations in temperature and pressure result in unwanted coupling within these high-dimensional DoFs in classical links (*23*–*27*) and a loss of entanglement for quantum channels (*28*–*33*) resulting in decreased performance and the loss of information. Numerical and digital technologies are widely used tools for investigating this problem, but only a handful of studies making use of real-world atmospheric channels (*34*–*39*).

Strategies to mitigate these effects have taken on many forms, including the use of adaptive optics (*40*–*42*), machine learning (*43*), modal diversity (*44*), and phase conjugation with nonlinear optics (*45*, *46*) to name a few. An alternative and exciting approach is to leverage the physics of atmospheric turbulence to find or create invariant forms of structured light, which can pass through medium as if it were transparent. These invariants can take many forms with recent studies including eigenmodes (*47*, *48*), optical knots (*49*), and the nonseparability of the vectorial beams (*50*, *51*) each with their own benefits and limitations. Optical skyrmions (*52*) are easy to generate, scale, measure, and bring to bear the many advantages of topology, where the mapping from real-space to a given parameter space is preserved, so long as the channel can be described as a smooth deformation of the map. It is not yet known which channels meet this criterion, and finding the channels that do is an active area of research. It has recently been demonstrated in controlled laboratory studies that classical skyrmions are robust to certain optical transformations (*53*), scattering media (*54*), and simulated atmospheric turbulence (*55*, *56*). Likewise, it has also been demonstrated that nonlocal quantum skyrmions are immune to the effects of entanglement decay (*57*) and isotropic noise (*58*). These studies used single phase screens and thus limited to only weak perturbations and did not venture to dynamic media with decoherence effects. To date, there has as yet been no demonstration of the robustness of any optical topology through realistic environments.

Here, we present results testing the stability of topological light through a real-world atmospheric channel. We prepare several optical skyrmions and transport them through a 270-m free-space optical link located on the Braamfontein campus of the University of the Witwatersrand, in the center of Johannesburg, South Africa. We measure the topology with a simple, single shot, spatially resolved Stokes polarimetry setup, allowing for the simultaneous measurement of all four Stokes parameters. We demonstrate that the topological wrapping number remains robust through the channel over a wide variety of atmospheric conditions, ranging from calm, cool morning air to the highly erratic and intense distortions of the midday heat. We first

[1]School of Physics, University of the Witwatersrand, Private Bag 3, Johannesburg 2050, South Africa. [2]University of Bordeaux, CNRS, Laboratoire Ondes et Matière d'Aquitaine, Talence, France. [3]School of Electrical and Information Engineering, University of the Witwatersrand, Private Bag 3, Johannesburg 2050, South Africa.
*Corresponding author. Email: andrew.forbes@wits.ac.za

present results of measurements made within the atmospheric coherence time τ_0, the timescale at which the medium appears transparent to the propagating beam and the typical upper limit for most classical communication schemes. We show that in this regime, the topological wrapping number is highly robust, being easily recovered even when the amplitude and phase distortions induced by the channel leave the underlying beam unrecognizable and the vectorial polarization structure highly scrambled. In addition, we also demonstrate the robustness of this topology to the decoherence and depolarization effects of turbulence, by averaging measurements over timescales greater than τ_0, allowing the experienced distortion to evolve during the measurement. These timescales are relevant when long measurement times are needed, for example, with slow detectors or when measuring single or biphoton states which require the buildup of statistics over time. Again, we show the preservation of the topological wrapping number despite an almost 40% drop in the beams degree of polarization (DoP). All measurements are performed with no probing of the medium and no pre- or postcorrection is made to compensate for the channel distortion. These results provide compelling evidence for the benefits of topological light and its potential to greatly improve the capacity of FSOC, both classical and quantum. They also motivate the development of new technologies for the effective and efficient generation and detection of topological light and open up exciting avenues for robust, correction-free optical communication and transmission through complex channels.

RESULTS

Creation and detection of optical skyrmions

We construct optical skyrmions of the form

$$\mathbf{U}(\mathbf{r}) = \mathrm{LG}_{l_1}^{0}(\mathbf{r})\mathbf{e}_R + \mathrm{LG}_{l_2}^{0}(\mathbf{r})\mathbf{e}_L \quad (1)$$

where $\mathrm{LG}_l^p(\mathbf{r})$ represents a Laguerre-Gaussian (LG) complex field, $\mathbf{r}$ is the transverse spatial coordinate, and $\mathbf{e}_{R(L)}$ represent the right (left) circular polarization unit vectors, respectively. We set the radial index of the LG beam to $p = 0$ for convenience and modulate the azimuthal index l to tune the topological wrapping number. This index imbues the beam with an orbital angular momentum (OAM) of $l\hbar$ per photon. States of this form are commonly referred to as vector beams (*59*, *60*) and exhibit complex, spatially varying polarization structures across the transverse plane. In the cases where $|l1| \neq |l_2|$, the spatially varying polarization structure, shown on the left hand side of Fig. 1, forms a skyrmionic topology. This mapping is characterized by a sphere-to-sphere mapping from the transverse plane $\mathcal{R}^2$ through a stereographic projection to the Poincaré sphere $\mathcal{S}^2$, shown by the mapping from the vector textured field in the transverse plane to the Poincaré sphere. Each skyrmionic topology is uniquely characterized by the topological wrapping number N, also called the skyrmion number. This integer value counts how many times one wraps the Poincaré sphere as one moves across the entire transverse plane (*52*). The wrapping number for a skyrmion formed using the three-dimensional Stokes vector field can be calculated as follows

$$N = \frac{1}{4\pi}\int_{\mathcal{R}^2} \boldsymbol{S}\cdot\left(\frac{\partial \boldsymbol{S}}{\partial x}\times\frac{\partial \boldsymbol{S}}{\partial y}\right)\mathrm{d}x\mathrm{d}y \quad (2)$$

where $\boldsymbol{S}$ is the locally normalized Stokes vector such that $\Sigma_{j=1}^{3}S_j^2 = 1$ to ensure the final mapping is always onto a unit sphere. For the above states, Eq. 2 simplifies to $N = n|l_1 - l_2|$, where $n = \mathrm{sign}(l_1 - l_2)$.

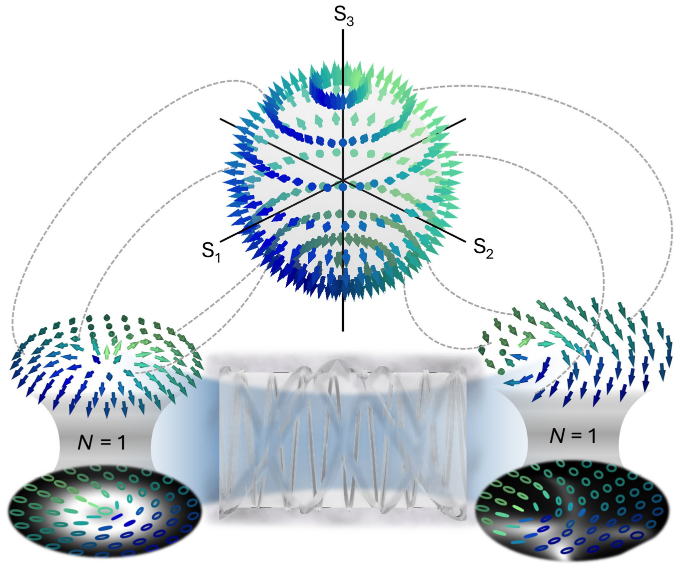

Fig. 1. Skyrmionic topology through turbulence. Illustration showing how optical skyrmions are formed via a mapping from the transverse plane to the Poincaré sphere, characterized by the skyrmion number N. When these states pass through a turbulent channel, the beam's structure is heavily distorted in phase, amplitude, and polarization, but the mapping to the Poincaré sphere is unchanged.

As illustrated in Fig. 1, when these states pass through atmospheric turbulence, the beam's amplitude profile and polarization structure are severely distorted, but the mapping from the transverse plane to the Poincaré sphere and, consequently, the topological wrapping number N are maintained.

Optical skyrmions were generated experimentally with the setup shown Fig. 2A. Here, a laser of wavelength 532 nm was shaped into various vectorial beams in the form of Eq. 1 with $l_1 = 1, 2$, and 3 and $l_2 = 0$ using a spatial light modulator (SLM) and a modified Mach-Zehnder interferometer, to generate optical skyrmions with $N = 1$, 2, and 3, respectively. These beams were then transmitted across a 270-m-long outdoor free-space link. At the receiver, a polarization sensitive camera and 50:50 beam splitter are used to measure the horizontal (H), vertical (V), diagonal (D), antidiagonal (A), right-circular (R), and left-circular (L) polarization intensity projections in a single shot similar to methods implemented in (*51*, *61*). Example projections taken for a skyrmion with $N = 1$ before and after propagation through the free-space link are shown in Fig. 2 (B and C), respectively. The simultaneous measurement of these projections is essential to ensure that the full state of polarization (SoP) of the beam is determined for a given atmospheric configuration within the coherence time of the channel. Appropriate optics have been used to ensure that the entire beam is collected, accounting for divergence and beam wander (see the Supplementary Materials), to ensure that the measurement itself is topology preserving. Figure 2 (D and E) shows the experimentally reconstructed SoP, Stokes vector texture, and the mapping onto the spatial sphere for optical skyrmions with $N = 1$ and $N = 2$ before propagating through the free-space link. Here, we clearly see how each distinct topology wraps a different number of times around the Poincaré sphere, and we can qualitatively evaluate the topology. For $N = 1$, the polarization states move from horizontal (blue) to vertical (green) only once and then back to horizontal as one moves azimuthally around the optical axis.

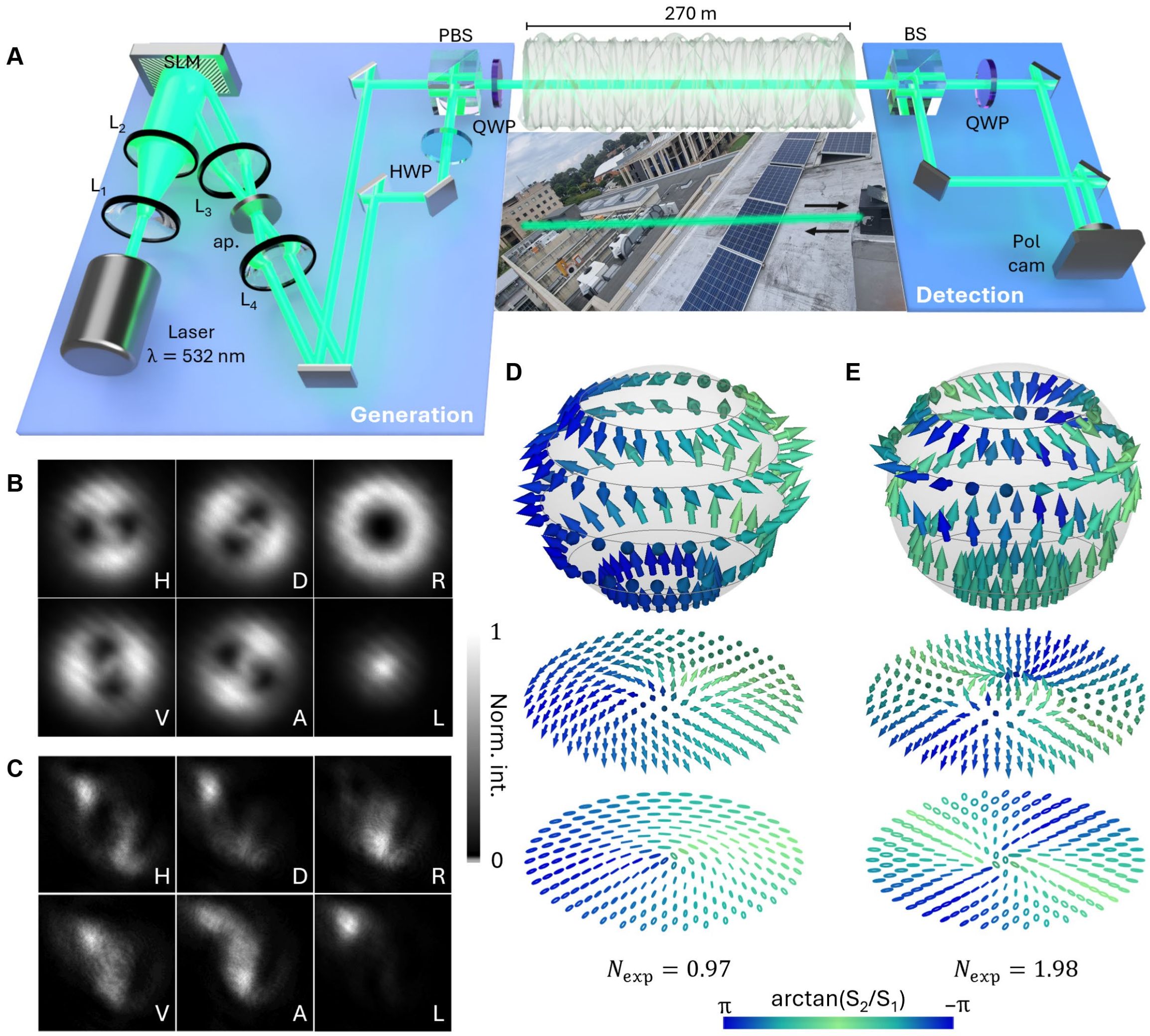

Fig. 2. Generation and detection through a free-space link. (**A**) Optical skyrmions were generated using complex amplitude holograms on a spatial light modulator (SLM) to generate two scalar modes. These modes were vectorially combined with a Mach-Zehnder interferometer and transmitted through a 270-m free-space optical link. At the receiver, Stokes polarimetry was performed on the aberrated beam using a 50:50 beam splitter, quarter-wave plate (QWP) and a polarization-sensitive camera (Pol. Cam.). (**B**) Polarization intensity projections for all six polarization states captures simultaneously for a skyrmion with $N = 1$ before the beam had propagated through the free-space link. (**C**) Polarization intensity projections for all six polarization states captures simultaneously for a skyrmion with $N = 1$ after the beam had propagated through the free-space link. (**D**) SoP, Stokes vector texture, and mapping to the spatial sphere for a unaberrated skyrmion beam with $N = 1$ captured using the detection scheme. (**E**) SoP, Stokes vector texture, and mapping to the spatial sphere for a unaberrated skyrmion beam with $N = 2$ captured using the detection scheme. PBS, polarizing beam splitter; HWP, half-wave plate; ap, aperture; BS, beam splitter.

This occurs twice in the SoP for $N = 2$. Quantitatively, the experimentally computed sphere coverage of $N_{exp} = 0.97$ and $N_{exp} = 1.98$ calculated using Eq. 2 is also extremely close to the encoded values indicating the successful generation and detection of the desired topologies before being exposed to turbulence.

Robustness through real-world free-space link

Figure 3A shows experimentally obtained intensities and SoPs for the skyrmions with $N = 1$ and $N = 2$ indoors (no turbulence) and through the free-space link in the morning, midday, and late afternoon. Morning weather conditions result in the least severe distortions, as seen by the only slight changes in the intensity profiles as compared to the indoor case, with the SoP roughly maintaining its cylindrical symmetry through the channel. These slight variations can be attributed to the phase distortions induced by the channel. Over and above this broken symmetry, we also see that most of the polarization states have changed in propagation. This is a result of a difference in the Gouy phase of the component scalar beams (*62*). In addition to a radius of curvature term, each LG beam gains a phase of $e^{i\psi(z)}$, where $\psi(z) = (2p+|l|+1)\arctan(z/z_R)$ and where z_R is the Rayleigh length of the beam. This phase depends on the mode order and thus the l-index of the scalar mode. Since the component modes of the vector beam must have differing l-indices to form the skyrmion mapping, the scalar components of each beam will accumulate phase at different rates, effectively having different propagation constants through free space. As a result, the polarization structure will change in propagation, even in the absence of a complex channel such as atmospheric turbulence. This effect does not

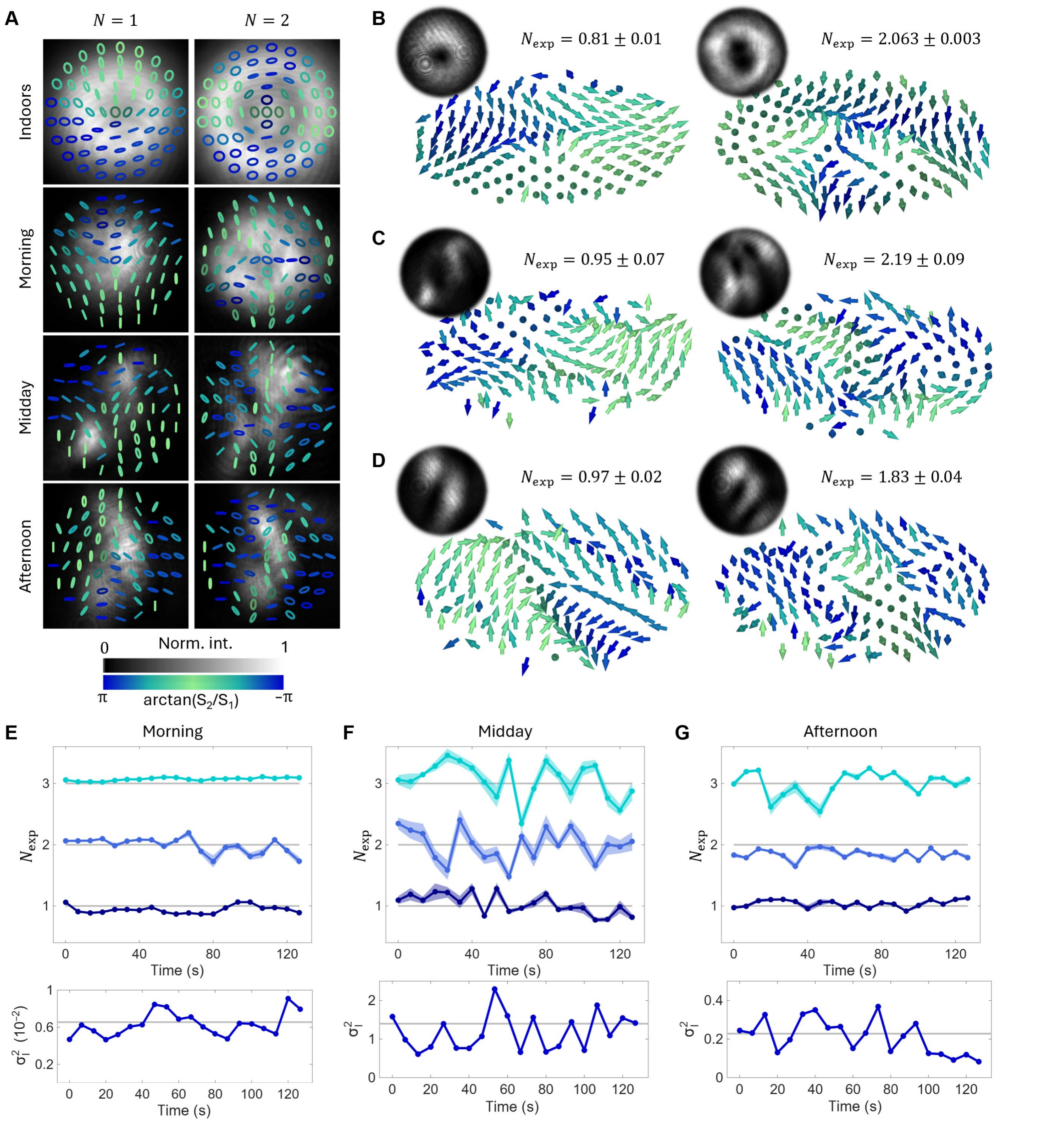

Fig. 3. Robustness through free-space link. (**A**) Total intensities and the measured SoP for skyrmion with $N = 1$ and $N = 2$ after propagating indoors and through the free-space link in the morning, midday, and late afternoon. Experimentally measured Stokes vector textures (main) and corresponding OAM scalar component (inset) for skyrmions transmitted in the (**B**) morning, (**C**) at midday, and (**D**) in the late afternoon. The measured skyrmion number for encoded numbers of $N = 1$, 2, and 3 and the measured scintillation index σ_I^2 measured over 120 s in the (**E**) morning, (**F**) at midday, and (**G**) in the late afternoon.

affect the skyrmion mapping and only changed the polarization texture. The data taken in the late afternoon show much more severe distortion in both amplitude and polarization. Here, we see that the intensity has lost its cylindrical symmetry, with highly distorted profiles. The SoP is also highly aberrated, with rapid variations in polarization across the transverse plane as compared to the smooth transitions seen in the SoP of the indoor data. The midday data show the most severe distortion, with separate lobes developing in the intensity profiles of the beams and far more rapid variations in the SoPs. The change in the severity of the distortion is easily explained by the changes in weather during the day. Morning temperatures start off quite low, with cool air and surfaces resulting in small temperature gradients and minimal turbulence. Midday sees the highest temperatures, heating up surrounding buildings, pavements, and roads and creating large temperature gradients ideal for creating very strong turbulence. By late afternoon, these surfaces begin to cool, leading to a decrease in the turbulence strength.

With a qualitative understanding of the distortion experienced at each of the three times of day, we may now quantify the topology after the beams have passed through the link at these different times. Figure 3B shows the computed Stokes vector texture for the morning data shown in Fig. 3A. The insets show the intensity of the scalar mode carrying OAM. We see that while the vector textures differ noticeably from the textures plotted in Fig. 2 (C and D), the topological features are maintained. The Stokes vector at the center still points upward, and the vectors rotate downward as one moves radially outward. For the $N = 1$ skyrmion, we see that the vectors rotate once around as we move azimuthally, indicating one wrapping around the Poincaré sphere and illustrated with the color map as moving from blue to green and back to blue only once. For the $N = 2$ skyrmion, this rotation occurs twice indicating two wrappings around the Poincaré sphere. These features agree well with the computed wrapping numbers of $N_{\mathrm{exp}} = 0.81 \pm 0.01$ and 2.063 ± 0.003, respectively. Figure 3C shows the computed Stokes vector texture for the midday data shown in Fig. 3A. Because of the severe distortion experienced at this time of day, the trends discussed previously are not as easy to visually discern from the plotted textures. However, we still see the single wrapping and double wrapping for $N = 1$ and $N = 2$, respectively, as one moves azimuthally. We also see good agreement between the encoded and measured skyrmion numbers of $N_{\mathrm{exp}} = 0.95 \pm 0.07$ and 2.19 ± 0.09, indicating robustness of the topology through even the most extreme cases tested. Figure 3D shows the computed Stokes vector texture for the afternoon data shown in Fig. 3A. Here, the distortion was milder than at midday but stronger than in the morning, with noticeable distortion in the vector textures. Despite this, we can still visually discern the single azimuthal wrapping for skyrmion $N = 1$ and double wrapping for $N = 2$. The experimentally evaluated values of the distorted beams of $N_{\mathrm{exp}} = 0.97 \pm 0.02$ and $N_{\mathrm{exp}} = 1.83 \pm 0.04$ again very closely match the encoded values.

We have established that the skyrmion number remains unchanged under specific instances of atmospheric turbulence, but it is important to study the robustness of this topology as the medium changes. We show the measured skyrmion number over ∼120 s in Fig. 3 (E to G) in the morning, at midday, and late afternoon respectively. We also show the measured scintillation indices σ_I^2 for the respective times of day, calculated using the variation of the on axis intensity $I(t)$ of left-circularly polarized component ($l_2 = 0$) of the transmitted beam according to (*22*)

$$\sigma_I^2 = \frac{\left\langle I^2(0,0,t)\right\rangle}{\left\langle I(0,0,t)\right\rangle^2} - 1 \tag{3}$$

where $\langle\cdot\rangle$ represents the average over time. Each data point shows the average measured skyrmion number over five sequential 2-ms measurements to allow for a measurement uncertainty to be determined. There were 6-s intervals between each data point and the shaded region indicating the measurement uncertainty. Atmospheric conditions in the morning showed an average scintillation index of $\sigma_I^2 \approx 0.007$, comparable to strengths seen in other free-space link experiments (*63*). This supports the qualitative evaluation made earlier, with only mild aberration seen in the beams' intensity profiles and SoPs. The skyrmion number for each of the tested topologies, $N = 1$, 2, and 3, remains fairly consistent over the measurement period, with only small fluctuations in the $N = 2$ topology in the second half of the measurement. The midday measurements show an average scintillation index of $\sigma_I^2 \approx 1.4$. This can be considered a very high value and corresponds well with the results in Fig. 3A. The measured skyrmion number over the measurement period is not as steady as seen in the morning data and fluctuates noticeably around the encoded value. However, despite these fluctuations, the value of each topology at almost every point in time is discernable from every other point and close enough to the encoded value to determine what the initially encoded topology was. It is worth noting that when the wrapping number is reported, it is calculated using Eq. 2 which gives the coverage of the Poincaré sphere. This coverage calculation can be prone to errors, especially in the presence of background noise, limited region of interest, and nonsymmetrical beam profiles. All of these factors are present in our measurements, and hence, we have taken appropriate numerical precautions to mitigate their effects in a manner that does not alter the inherent topology (see the Supplementary Materials) (*64*). Despite these challenges, we are able to easily distinguish between various encoded topologies even in the most extreme cases through the real-world free-space link. The afternoon data show smaller variation over the measurement period for all three encoded topologies as compared to the midday data but more severe than the morning data, with an average distortion strength of $\sigma_I^2 \approx 0.23$. This again aligns with the qualitative observations discussed earlier, over this measurement period. Here, we again see that the measured skyrmion number fluctuates over the course of the measurement but still remains close to the encoded value, allowing us to easily identify what the transmitted topology was through the distorting channel. The robustness of the topology is in stark contrast to how OAM itself performs, showing decreased fidelity, high cross-talk, and significant modal scattering (see the Supplementary Materials).

Resilience to depolarization and decoherence in turbulence

So far, we have discussed the robustness of optical skyrmions to atmospheric phase distortions and the scintillations that results from these. The measurements were taken over short measurement times and did not allow the channel to significantly evolve during the acquisition time for each data point. In the context of classical optical communications, this robustness is vital for reliable and effective data transmission. However, skyrmions have also recently been realized in the quantum domain, for both single photon states (*65*) and in hybrid entangled biphoton states (*57*), promising increased security and data protection for quantum communication. Measurement of quantum states requires significantly longer measurement times, with even the most state of the art techniques requiring measurement times on the order of $\approx 10^2$ s (*66*). Typical atmospheric coherence times are on the order of 10 to 100 ms (*67*). Therefore, quantum states sent through turbulence will undergo multiple realizations of the channel over the course of a single measurement, leading to additional deleterious effects caused by depolarization and decoherence. Several experiments have simulated the effects of these channels on optical skyrmions, with promising results demonstrating possible resilience (*68*). Here, we have a unique opportunity to study this phenomenon in a real-world channel. Using classical light, we can easily probe the effects of depolarization and decoherence, with the results being directly transferable to quantum skyrmions due to the close mathematical analogy between hybrid entangled biphoton states and classical vector beams (*60*, *69*, *70*). We show our results in Fig. 4. The first row of Fig. 4A shows the normalized total intensity and Stokes parameters for a skyrmion with $N = 1$ under indoor conditions, with no turbulence. We see that the Stokes parameters are unaberrated, and the DoP is close to 1, meaning that the beam is almost fully polarized and coherent. The second row of Fig. 4A shows the Stokes parameters for the same beam but now after a 2-ms exposure time through the turbulence channel. The Stokes parameters are distorted, but the beams DoP is still relatively high, having decreased primarily because of the presence of ambient, thermal light such as sunlight. The third row of Fig. 4A shows the Stokes parameters for a beam after averaging for 25 ms. Here, we can see that the magnitudes of the parameters have decreased as compared to the second row. The DoP of this state is 0.59, indicating that a portion of the field measured is now partially incoherent/depolarized. However, the computed skyrmion number still remains close to the encoded value of $N = 1$. The fourth row of Fig. 4A shows the Stokes parameters for the same beam after averaging for even longer, 120 ms. Here, we see that the amplitudes of the Stokes parameters have decreased even further, indicating even more severe depolarization. This is further supported by the calculated DoP for this state, which is 0.39. The measured wrapping number for this beam is $N = 0.98$, still close to the encoded value. Figure 4B shows the measured skyrmion number for $N = 1$, 2, and 3 as the measurement was averaged over longer and longer time periods. Figure 4C plots the DoP over averaging time, indicating the severity of the effect of the depolarization during the course of the measurement. We see that the skyrmion number remains almost perfectly unchanged for all three encoded values from the initial exposure time of 2 ms up to a total time of 240 ms (2-ms exposure per image averaged over 120 images). This is despite the fact that the DoP drops from ≈0.84 to ≈0.39, a significant decrease over the course of the measurement. This shows that optical skyrmions are immune to the effects of decoherence and depolarization caused by real-world atmospheric turbulence.

Robust information transfer in atmospheric turbulence

We have now seen that optical skyrmions are resilient to a wide variety of turbulence channels. One promising applications for this is robust information encoding through free space. Atmospheric turbulence typically distorts more common forms of structured lights, leading to severe cross-talk if no compensation techniques are used to mitigate its effects. In contrast, the wrapping number of the generated optical skyrmions typically remains unchanged through these channels, meaning that it can safely encode data through the link. We demonstrate this experimentally by way of visual example shown in Fig. 5. Here, we encode a three-color, 512 by 560 image of South Africa using topology, where each N corresponds to a particular color, with $N = 1$, 2, and 3 corresponding to blue, orange, and green respectively. We then transmit the image one pixel at a time over a time interval of 2 ms with the appropriate topological state being transmitted through the channel and measured at the receiver. The received image is constructed by measuring the skyrmion number of the received state. If fractional values are measured, then they are rounded off to the nearest integer. Figure 5A shows the results taken in the morning, with the line graph showing examples of the individual measured skyrmion numbers during measurement period and the shaded region indicating the mean ± one SD. As before, the variation in the measured number during the morning is minor, with only a few data points for $N = 2$ deviating noticeably. The reconstructed

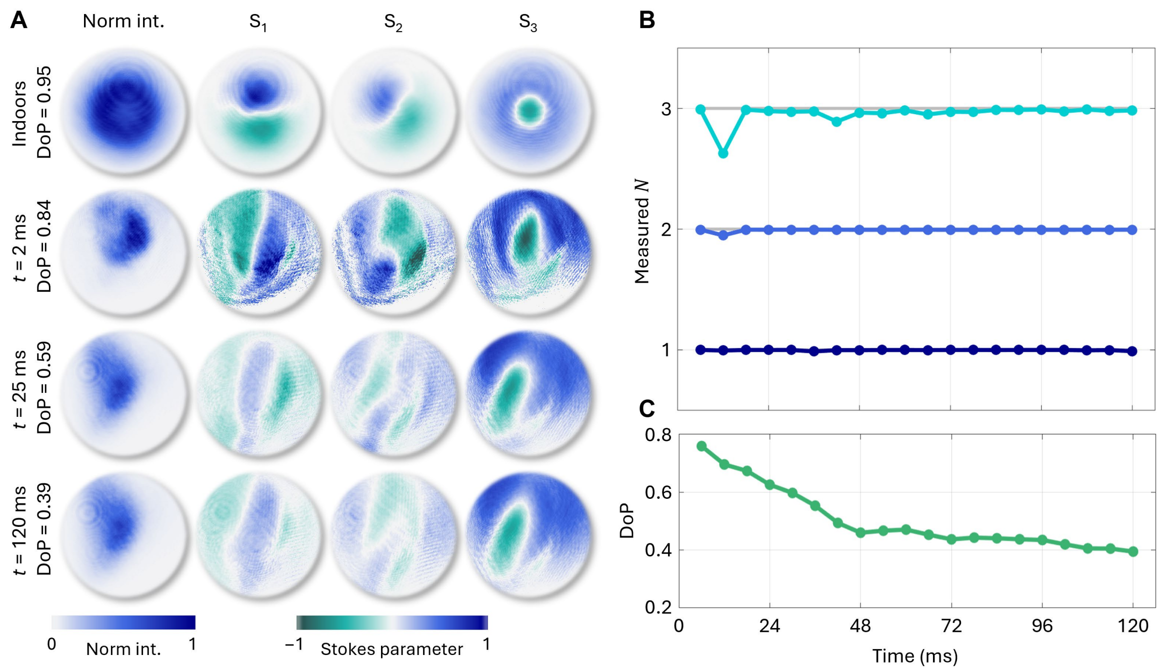

Fig. 4. Resilience to depolarization and decoherence. (**A**) The measured intensity and locally normalized Stokes parameters of a skyrmion beam with $N = 1$ measured indoors (top row), after averaging for 2 ms (second row), after averaging for 25 ms (third row), and after averaging for 120 ms (fourth row). (**B**) Line plot showing the measured skyrmion number for encoded numbers of $N = 1$, 2, and 3 against the time over which the measurement was averaged. (**C**) Line plot showing the measured DoP against the time over which the measurement was averaged.

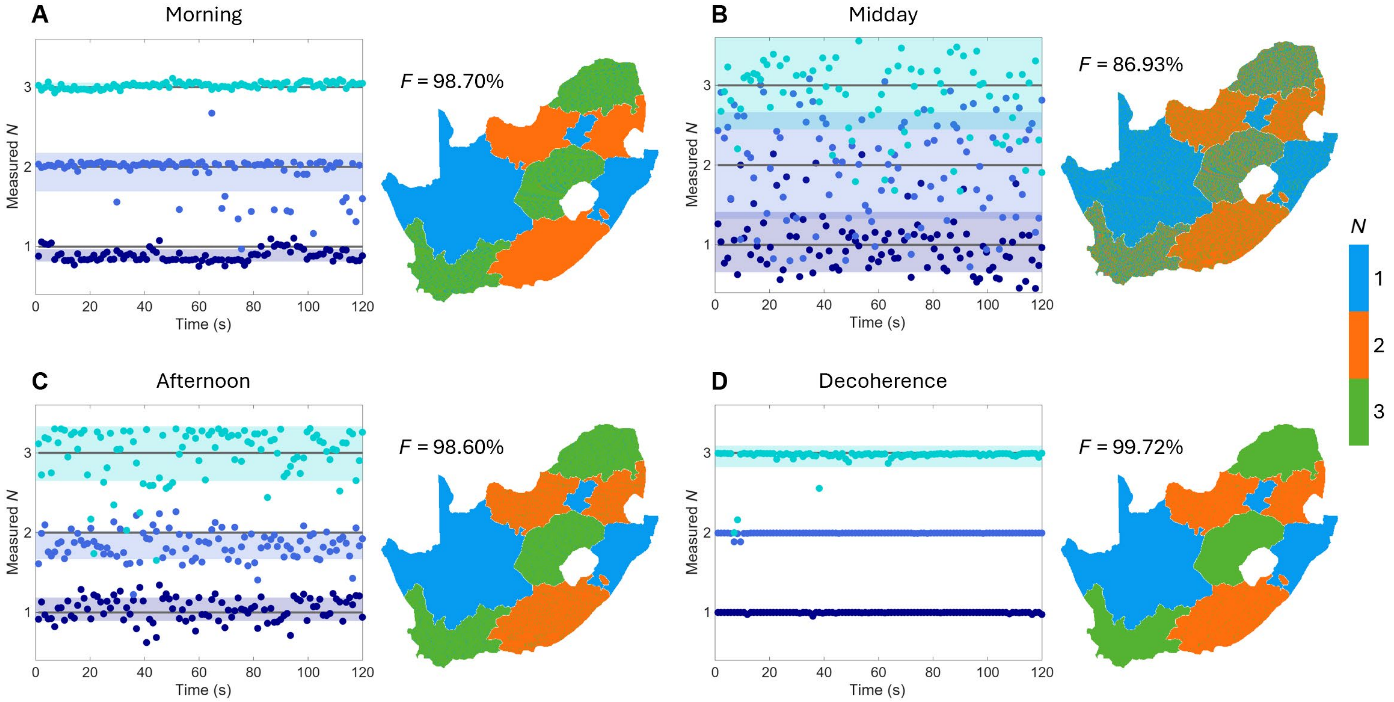

Fig. 5. Robust information encoding. The measured skyrmion numbers over the measurement period and the reconstructed image of the transmitted image performed (**A**) in the morning under mild distortion, (**B**) at midday during the most severe distortion conditions, (**C**) in the late afternoon under moderate distortion, and (**D**) under the effects of increasing depolarization.

image maintains its structure, with each province in the map maintaining a uniform, unaltered color indicating that the information was transmitted with an almost perfect fidelity of 98.70%. Figure 5B shows results taken at midday, exhibiting significant deviations from the encoded value due to the significant turbulence strength experienced during this time of day. We see this quantitatively with the reconstructed image having a fidelity of 86.93%. We do see some noticeable discoloration in the reconstructed image as a result of this, especially for the higher-order topologies of $N = 2$ and 3. However, the various regions in the reconstructed image are still discernable from each other, and the initial encoded color is still easily identifiable. Figure 5C shows the results taken in the afternoon. We see that the variation is higher than in the morning but less than at midday. There are some slight errors for the $N = 2$ topology, evident by the presence of some green pixels in regions which are orange in the encoded image, but overall, the image integrity was well maintained through the channel, seen with a fidelity of 98.60%. Figure 5D shows the same data but under the condition where the measurement is averaged over 240 ms in turbulence to allow for there to be significant depolarization in the same regime as Fig. 4. In this case, the fidelity is extremely high at 99.72%. We see almost no variation in the measured N due to fact that averaging the measurement also averages over the effects of the ambient light and shot noise of the camera, reducing its deleterious effects on the wrapping number calculation. Overall, we see that topology makes a useful alphabet for transmitting information through the free-space link, only showing a noticeable drop in performance in the most extreme cases, where the distortion is severe. However, even in this regime, without any measurement or probing of the channel or pre- or postcompensation, the image is able to be transmitted with a reasonably high fidelity.

It is worth noting that skyrmion states of different N are not, in general, spatially orthogonal to one another, so our scheme does not constitute mode-division multiplexing in the conventional sense. Instead, we use an index modulation approach: At each symbol interval, one skyrmion state is transmitted, and the receiver identifies which state was sent, much like selecting one symbol from an alphabet. The relevant requirement is therefore that the states be sufficiently distinguishable from one another at the receiver, not that they be mutually orthogonal. This is a well-established principle in wireless communications, for example, modern Multiple-Input-Multiple-Output (MIMO) systems (such as those in everyday Wi-Fi routers with multiple antennas) routinely operate with nonorthogonal spatial channels and rely on signal processing at the receiver to separate them. In principle, multiple skyrmion states could also be copropagated simultaneously to form a full multiplexing scheme, although this would require appropriate detection strategies to manage interchannel cross-talk, for instance, successive interference cancellation (SIC) (*71*), where the receiver decodes the strongest channel first, subtracts its contribution, and iterates to recover the remaining channels. Regarding turbulence robustness, since our results show that individual skyrmion states preserve their topological structure through turbulence, the distinguishability needed for index modulation is maintained. We therefore expect that a SIC-based multiplexing scheme would inherit much of this robustness, although quantifying the cross-talk penalty under realistic turbulence strengths remains an open question for future investigation. Note also that the skyrmion numbers could be made orthogonal by careful choice of constituent modes, so MDM could be done with them too.

DISCUSSION

Experiments so far have primarily focused on the generation of optical skyrmions and other forms of topological light, with only a few recent works investigating their robustness through complex channels. These investigations, while valuable, were performed in controlled laboratory settings. In this work, we have presented experimental evidence of the robustness of optical skyrmions through a real-world turbulent channel. We have shown that the topology is preserved under the phase, amplitude, and polarization distortions imparted onto any light field that passes through such a channel. This was demonstrated over a wide variety of conditions, ranging from morning to midday and late afternoon, where the strength of the experienced turbulence varied from $\sigma_I^2 \approx 0.007$ to $\sigma_I^2 \approx 1.4$. We also demonstrated the invariance of the skyrmionic topology to the decoherence and depolarization effects that are typically observed when averaging over the time varying effects of the turbulence channel. Here, the skyrmion number remains unchanged even when the DoP dropped to as low as 0.39. In both cases, the robustness was achieved by harnessing properties of the light itself to generate structures that are invariant to actions of the channel. This is in contrast to many other proposed solutions to the issue of atmospheric turbulence, which either require a form of pre- or postcompensation such as adaptive optics or require a probe or measurement of the channel, such as finding its invariant spatial mode. Here, the invariant passes through the channel as if it was transparent, and no knowledge of the channel is required.

The use of topology also has benefits and trade-offs over similar approaches to finding and leveraging invariants, such as using the nonseparability of vectorial beams (*50*). While the nonseparability of vectorial light can be measured using integrated intensity measurements, making it easier and faster to detect with current technologies, it is susceptible to noise at lower values and requires the channel to be unitary. This is the case for the phase and amplitude distortions but does not occur when one experiences decoherence/depolarization (*72*). Skyrmionic topologies, on the other hand, do not require the channel to be unitary, only that it be map preserving which is typically an easier condition to satisfy (*68*).

Structured light in real-world atmospheric turbulence has seen only a handful of tests. This is primarily due to the difficultly in setting up free-space links capable of producing and detecting structured modes. These channels lack tunability and control while adding many confounding factors such as ambient noise, natural misalignment, and rapidly changing distortions to name a few. While these many considerations make these investigations challenging to undertake, they are also precisely why these investigations are valuable. We have shown in this work that the use of topology as an information carrier not only overcomes the fundamental physical limitations hampering both classical and quantum FSOC (i.e., mode coupling and decoherence) but also mitigates some of the more practical restrictions placed on these systems by misalignment, background noise, and the need for adaptive optics.

It is worth noting that in this investigation, we made use of a polarization camera and Stokes polarimetry to measure the skyrmion number. In the absence of a dedicated topological detector, such means are now the best available tools for this purpose. However, this method has two primary shortcomings for real-world implementation. First, it is prone to errors and fluctuations when computing the wrapping number, especially in the presence of high ambient noise such as sunlight and differing path lengths for different polarization projections in experiment (*64*). While these factors can be mitigated to a certain degree, sometimes through more sophisticated measurement schemes (*73*), they can never be fully removed resulting in noticeable fluctuations in the measured data. Second, high-speed modulation and detection with the scheme used in this work are challenging, due to the relatively low refresh rate of the SLM (120 Hz) and camera acquisition time (2 ms). For high-speed generation and modulation, the transmission architecture could mirror that of OAM-based systems: A conventional high-speed modulator (e.g., a Mach-Zehnder modulator operating at gigahertz rates) drives the data stream, followed by a static beam-shaping element that imposes the desired skyrmion structure. Devices such as J-plates (*74*), metasurfaces (*75*, *76*), or q-plates (*77*) could replace the SLM and would not limit the modulation bandwidth. The more significant bottleneck lies at the receiver. Unlike OAM, for which mode sorters based on log-polar transformations exist (*78*), there is now no analogous sorter for skyrmion states. Detection therefore requires either full Stokes polarimetry with spatial resolution or with single shot-projective metasurfaces (*79*) followed by computational classification or the development of dedicated optical elements that can efficiently separate skyrmion states—a skyrmion mode sorter that is yet to be fully realized (*80*). These devices would be key enablers for bringing skyrmion-based communication to data rates competitive with existing structured-light schemes. Our work demonstrates the potential for using skyrmions and other exotic forms of topological light as information encoders, inspiring future research into methods for faster and more effective detectors, paving the way for high-speed communication through complex media using robust topologies.

In this work, we generated optical skyrmions using specific combinations of LG beams with the same embedded Gaussian beam waist w_0. This means that higher-order topologies experienced stronger turbulence strengths, due to the inherent scaling of LG transverse beam size with OAM (*81*). Hence, a fair comparison of robustness of topologies with different N cannot be made with these results and is an open questions that merits further investigations. In addition, skyrmions in this work were made by setting $l_2 = 0$ and modulating l_1 to change N, Different combinations of l_1 and l_2 can result in the generation of beams with different underlying spatial modes but the same N. Optimizing the underlying geometry of topological light to increase its robustness has already shown promise for optical knots (*49*). It may therefore be of interest for future studies to investigate whether other vectorial combinations of LG beams, forming skyrmions with the same N tested here, could offer even greater resilience to the aberrations induced by complex channels.

The generation of skyrmions from LG beams with same embedded Gaussian waist w_0 implies that each beam has the same Rayleigh range and comparable propagation dynamics. Consequently, higher-order skyrmions must have a larger spatial extent due the ℓ-dependent scaling of the underlying LG modes (*81*). To normalize the beam sizes would mean that higher-order skyrmions diverge faster in propagation, making their dynamics significantly more challenging to unify through a single link, especially over a distance as large as the one used in this experiment. This also means that beams will have the same size at the transmitter but would still be different as they propagate through the link as it is a thick, extended medium. The modeling of structured beams in such scenarios has seen little attention in the literature and is a far more complex problem than simply ensuring the beam sizes are the same at a particular plane. However, one can engineer the beam sizes to be similar. For instance, rather than $\ell_1 = 0$

and $\ell_2 = 5$ as the two component scalar modes, one could select $\ell_1 = -2$ and $\ell_2 = 3$, which have similar sizes. It is also worth recalling that opposite signs of N, even at fixed $|N|$, necessarily correspond to distinct field structures. This provides a simple counterexample to the idea that identical spatial footprints would imply identical topology: Two configurations may share the same overall spatial extent while remaining topologically inequivalent. Even more efficient in this regard is to create very high skyrmion modes using perfect vortex structures with nearly identical spatial overlap, as has been shown recently (*82*), whose transverse intensity distribution is independent of the topological charge. The underlying idea is relevant here as it refers to a family of fields in which the spatial footprint remains invariant while the topological invariant changes. This tells that working with different N does not necessarily come with footprint drawbacks. However, our main point is that topology is a global property that is unrelated to its underlying structure. That is to say, from a topological perspective, all beams of a given N belong to an equivalence class defined by their skyrmion number, and because the channel is map preserving, it simply transforms the beam from one element of that class to another.

Robustness to phase and amplitude distortions resulting from turbulence, as well as the resilience to decoherence, is of immense interest to the field of free-space optical communication, where the search for a reliable, resilient, and high-dimensional encoding alphabet has the potential to markedly increase bandwidths and data transfer speeds. We have demonstrated in this work not only the robustness of these topological states to this highly complex medium but also their ability to faithfully transmit data through such channels with ease. We envision that our results will pave the way towards seeing and transporting information through distortion by harnessing light's innate, invariant properties for fast, reliable, and efficient communication.

METHODS

A diagram of the experimental setup used in this work can be seen in Fig. 2A. Here, a green laser beam ($\lambda = 532$ nm) was expanded using a 10× objective lens L_1 and collimated with a second lens L_2 of focal length $f_2 = 500$ mm. This beam was then incident on a PLUTO-VIS HoloEye SLM. The SLM screen was split in half, with each half generating one component scalar mode of the final vectorial beam using a complex amplitude modulation scheme (*83*)

$$H(x,y) = J_1^{-1}[A(x,y)]\sin\left[\phi(x,y) + 2\pi\left(G_x x + G_y y\right)\right] \quad (4)$$

where $A(x,y)$ and $\phi(x,y)$ are the amplitude and phase of the desired field, respectively, J_1^{-1} is the inverse Bessel function of the first kind, and $G_{x(y)}$ are the grating frequencies in the horizontal and vertical directions. Both beams are created with an embedded Gaussian beam waist of $w_0 = 0.665$ mm and are sent through a 4f imaging system consisting of lenses L_3 and L_4 (focal lengths $f_3 = f_4 = 300$ mm) with an iris in between acting as a spatial filter to isolate the first diffraction order of the hologram where our encoded scalar fields are located. These beams are propagating, but not coaxial, and are thus sent through a modified Mach-Zehnder interferometer, with a half-wave plate in one arm, to form the desired vectorial beam with the aid of a polarizing beam splitter. Before it is transported through the free-space link, the vectorial beam is sent through a quarter-wave plate (QWP) to convert the scalar component modes to the right- and left-circular polarization basis. It is then sent through two further telescope systems, each providing a further ×3 magnification such that the beam transmitted through the free-space link has an embedded Gaussian beam waist of $w_0 = 6$ mm. The telescope systems are constructed such that the beam focuses on a flat mirror fixed on the top of the opposite building, located ∼135 m from the last telescope system, for a round trip distance 270 m. Upon returning to the receiver, which is offset from the transmitter by roughly 60 cm to create a triangular beam path, the beam is demagnified by a telescope system with a ×0.125 magnification and then incident on a 50:50 beam splitter. One port of the beam splitter leads directly to one half of the sensor of a polarization sensitive camera (Allied vision Mako G-508B POL) to measure the four linear polarization states: horizontal, vertical, diagonal, and antidiagonal. The other port of the beam splitter passes through a QWP before being incident on the other half of the camera sensor to measure the right- and left-circular polarization states.

Supplementary Materials

The PDF file includes:

Supplementary Text
Figs. S1 to S5
Legend for data S1
References

Other Supplementary Material for this manuscript includes the following:

Data S1

REFERENCES

1. T. Richter, E. Palushani, C. Schmidt-Langhorst, R. Ludwig, L. Molle, M. Nolle, C. Schubert, Transmission of single-channel 16-qam data signals at terabaud symbol rates. *J. Lightwave Technol.* **30**, 504–511 (2012).
2. A. Sano, H. Masuda, T. Kobayashi, M. Fujiwara, K. Horikoshi, E. Yoshida, Y. Miyamoto, M. Matsui, M. Mizoguchi, H. Yamazaki, Y. Sakamaki, H. Ishii, Ultra-high capacity wdm transmission using spectrally-efficient pdm 16-qam modulation and c-and extended l-band wideband optical amplification. *J. Lightwave Technol.* **29**, 578–586 (2011).
3. X. Zhou, J. Yu, M.-F. Huang, Y. Shao, T. Wang, L. Nelson, P. Magill, M. Birk, P. I. Borel, D. W. Peckham, R. Lingle Jr., B. Zhu, 64-tb/s, 8 b/s/hz, pdm-36qam transmission over 320 km using both pre- and post-transmission digital signal processing. *J. Lightwave Technol.* **29**, 571–577 (2011).
4. A. H. Gnauck, P. J. Winzer, S. Chandrasekhar, X. Liu, B. Zhu, D. W. Peckham, Spectrally efficient long-haul wdm transmission using 224-gb/s polarization-multiplexed 16-qam. *J. Lightwave Technol.* **29**, 373–377 (2011).
5. D. J. Richardson, Filling the light pipe. *Science* **330**, 327–328 (2010).
6. M. P. J. Lavery, M. M. Abadi, R. Bauer, G. Brambilla, L. Cheng, M. A. Cox, A. Dudley, A. D. Ellis, N. K. Fontaine, A. E. Kelly, C. Marquardt, S. Matlhane, B. Ndagano, F. Petruccione, R. Slavík, F. Romanato, C. Rosales-Guzmán, F. S. Roux, K. Roux, J. Wang, A. Forbes, Tackling africa's digital divide. *Nat. Photonics* **12**, 249–252 (2018).
7. A. Trichili, M. A. Cox, B. S. Ooi, M.-S. Alouini, Roadmap to free space optics. *J. Opt. Soc. Am. B* **37**, A184–A201 (2020).
8. A. Forbes, M. De Oliveira, M. R. Dennis, Structured light. *Nat. Photonics* **15**, 253–262 (2021).
9. X. Liu, S. Chandrasekhar, X. Chen, P. J. Winzer, Y. Pan, T. F. Taunay, B. Zhu, M. Fishteyn, M. F. Yan, J. M. Fini, E. M. Monberg, F. V. DiMarcello, 112-Tb/s 32-qam-ofdm superchannel with 86-b/s/Hz intrachannel spectral efficiency and space-division multiplexed transmission with 60-b/s/hz aggregate spectral efficiency. *Opt. Express* **19**, B958–B964 (2011).
10. G. Li, N. Bai, N. Zhao, C. Xia, Space-division multiplexing: The next frontier in optical communication. *Adv. Opt. Photonics* **6**, 413–487 (2014).
11. D. J. Richardson, J. M. Fini, L. E. Nelson, Space-division multiplexing in optical fibres. *Nat. Photonics* **7**, 354–362 (2013).
12. S. Berdagué, P. Facq, Mode division multiplexing in optical fibers. *Appl. Optics* **21**, 1950–1955 (1982).
13. G. Gibson, J. Courtial, M. J. Padgett, M. Vasnetsov, V. Pas'ko, S. M. Barnett, S. Franke-Arnold, Free-space information transfer using light beams carrying orbital angular momentum. *Opt. Express* **12**, 5448–5456 (2004).

14. I. B. Djordjevic, Deep-space and near-earth optical communications by coded orbital angular momentum (oam) modulation. *Opt. Express* **19**, 14277–14289 (2011).
15. H. Rubinsztein-Dunlop, A. Forbes, M. V. Berry, M. R. Dennis, D. L. Andrews, M. Mansuripur, C. Denz, C. Alpmann, P. Banzer, T. Bauer, E. Karimi, L. Marrucci, M. Padgett, M. Ritsch-Marte, N. M. Litchinitser, N. P. Bigelow, C. Rosales-Guzmán, A. Belmonte, J. P. Torres, T. W. Neely, M. Baker, R. Gordon, A. B. Stilgoe, J. Romero, A. G. White, R. Fickler, A. E. Willner, G. Xie, B. McMorran, A. M. Weiner, Roadmap on structured light. *J. Opt.* **19**, 013001 (2017).
16. I. Nape, B. Sephton, P. Ornelas, C. Moodley, A. Forbes, Quantum structured light in high dimensions. *APL Photonics* **8**, 051101 (2023).
17. Y. Shen, Rays, waves, su (2) symmetry and geometry: Toolkits for structured light. *J. Opt.* **23**, 124004 (2021).
18. S. Yoon, M. Kim, M. Jang, Y. Choi, W. Choi, S. Kang, W. Choi, Deep optical imaging within complex scattering media. *Nat. Rev. Phys.* **2**, 141–158 (2020).
19. C. He, H. He, J. Chang, B. Chen, H. Ma, M. J. Booth, Polarisation optics for biomedical and clinical applications: A review. *Light Sci. Appl.* **10**, 2028–2047 (2021).
20. V. Ntziachristos, Going deeper than microscopy: The optical imaging frontier in biology. *Nat. Methods* **7**, 603–614 (2010).
21. H. Cao, T. Čižmár, S. Turtaev, T. Tyc, S. Rotter, Controlling light propagation in multimode fibers for imaging, spectroscopy, and beyond. *Adv. Opt. Photonics* **15**, 524–612 (2023).
22. C. Peters, V. Cocotos, A. Forbes, Structured light in atmospheric turbulence–a guide to its digital implementation: Tutorial. *Adv. Opt. Photonics* **17**, 113–184 (2025).
23. J. A. Anguita, M. A. Neifeld, B. V. Vasic, Turbulence-induced channel crosstalk in an orbital angular momentum-multiplexed free-space optical link. *Appl. Optics* **47**, 2414–2429 (2008).
24. B. Rodenburg, M. P. J. Lavery, M. Malik, M. N. O'Sullivan, M. Mirhosseini, D. J. Robertson, M. Padgett, R. W. Boyd, Influence of atmospheric turbulence on states of light carrying orbital angular momentum. *Opt. Lett.* **37**, 3735–3737 (2012).
25. L. Zhang, F. Shen, B. Lan, A. O. Tang, Mode-dependent crosstalk and detection probability of orbital angular momentum of optical vortex beam through atmospheric turbulence. *J. Opt.* **22**, 075607 (2020).
26. C. Paterson, Atmospheric turbulence and orbital angular momentum of single photons for optical communication. *Phys. Rev. Lett.* **94**, 153901 (2005).
27. M. A. Cox, L. Maqondo, R. Kara, G. Milione, L. Cheng, A. Forbes, The resilience of hermite–and laguerre–gaussian modes in turbulence. *J. Lightwave Technol.* **37**, 3911–3917 (2019).
28. A. K. Jha, G. A. Tyler, R. W. Boyd, Effects of atmospheric turbulence on the entanglement of spatial two-qubit *states*. *Phys. Rev. A* **81**, 053832 (2010).
29. A. Hamadou Ibrahim, F. S. Roux, M. McLaren, T. Konrad, A. Forbes, Orbital-angular-momentum entanglement in turbulence. *Phys. Rev. A* **88**, 012312 (2013).
30. C. Gopaul, R. Andrews, The effect of atmospheric turbulence on entangled orbital angular momentum states. *New J. Phys.* **9**, 94 (2007).
31. B.-J. Pors, C. H. Monken, E. R. Eliel, J. P. Woerdman, Transport of orbital-angular-momentum entanglement through a turbulent atmosphere. *Opt. Express* **19**, 6671–6683 (2011).
32. N. D. Leonhard, V. N. Shatokhin, A. Buchleitner, Universal entanglement decay of photonic-orbital-angular-momentum qubit states in atmospheric turbulence. *Phys. Rev. A* **91**, 012345 (2015).
33. G. Sorelli, N. Leonhard, V. N. Shatokhin, C. Reinlein, A. Buchleitner, Entanglement protection of high-dimensional states by adaptive optics. *New J. Phys.* **21**, 023003 (2019).
34. M. Krenn, R. Fickler, M. Fink, J. Handsteiner, M. Malik, T. Scheidl, R. Ursin, A. Zeilinger, Communication with spatially modulated light through turbulent air across vienna. *New J. Phys.* **16**, 113028 (2014).
35. M. Krenn, J. Handsteiner, M. Fink, R. Fickler, R. Ursin, M. Malik, A. Zeilinger, Twisted light transmission over 143 km. *Proc. Natl. Acad. Sci. U.S.A.* **113**, 13648–13653 (2016).
36. Y. Ren, Z. Wang, P. Liao, L. Li, G. Xie, H. Huang, Z. Zhao, Y. Yan, N. Ahmed, A. Willner, M. P. J. Lavery, N. Ashrafi, S. Ashrafi, R. Bock, M. Tur, I. B. Djordjevic, M. A. Neifeld, A. E. Willner, Experimental characterization of a 400 gbit/s orbital angular momentum multiplexed free-space optical link over 120 m. *Opt. Lett.* **41**, 622–625 (2016).
37. M. P. J. Lavery, C. Peuntinger, K. Günthner, P. Banzer, D. Elser, R. W. Boyd, M. J. Padgett, C. Marquardt, G. Leuchs, Free-space propagation of high-dimensional structured optical fields in an urban environment. *Sci. Adv.* **3**, e1700552 (2017).
38. M. Krenn, J. Handsteiner, M. Fink, R. Fickler, A. Zeilinger, Twisted photon entanglement through turbulent air across vienna. *Proc. Natl. Acad. Sci. U.S.A.* **112**, 14197–14201 (2015).
39. A. Sit, F. Bouchard, R. Fickler, J. Gagnon-Bischoff, H. Larocque, K. Heshami, D. Elser, C. Peuntinger, K. Günthner, B. Heim, C. Marquardt, G. Leuchs, R. W. Boyd, E. Karimi, High-dimensional intracity quantum cryptography with structured photons. *Optica* **4**, 1006–1010 (2017).
40. R. K. Tyson, Bit-error rate for free-space adaptive optics laser communications. *J. Opt. Soc. Am. A* **19**, 753–758 (2002).
41. S. M. Zhao, J. Leach, L. Y. Gong, J. Ding, B. Y. Zheng, Aberration corrections for free-space optical communications in atmosphere turbulence using orbital angular momentum states. *Opt. Express* **20**, 452–461 (2012).
42. Y. Ren, G. Xie, H. Huang, N. Ahmed, Y. Yan, L. Li, C. Bao, M. P. J. Lavery, M. Tur, M. A. Neifeld, R. W. Boyd, J. H. Shapiro, A. E. Willner, Adaptive-optics-based simultaneous pre- and post-turbulence compensation of multiple orbital-angular-momentum beams in a bidirectional free-space optical link. *Optica* **1**, 376–382 (2014).
43. J. Liu, P. Wang, X. Zhang, Y. He, X. Zhou, H. Ye, Y. Li, X. Shixiang, S. Chen, D. Fan, Deep learning based atmospheric turbulence compensation for orbital angular momentum beam distortion and communication. *Opt. Express* **27**, 16671–16688 (2019).
44. M. A. Cox, L. Cheng, C. Rosales-Guzmán, A. Forbes, Modal diversity for robust free-space optical communications. *Phys. Rev. Appl.* **10**, 024020 (2018).
45. S. Singh, B. Sephton, W. T. Buono, V. D'Ambrosio, T. Konrad, A. Forbes, Light correcting light with nonlinear optics. *Adv. Photonics* **6**, 026003 (2024).
46. H. Zhou, S. Xinzhou, Y. Duan, Y. Zuo, Z. Jiang, M. Ramakrishnan, J. Tepper, V. Ziegler, R. W. Boyd, M. Tur, A. E. Willner, Automatic mitigation of dynamic atmospheric turbulence using optical phase conjugation for coherent free-space optical communications. *Optica* **12**, 158–167 (2025).
47. A. Klug, C. Peters, A. Forbes, Robust structured light in atmospheric turbulence. *Adv. Photonics* **5**, 016006 (2023).
48. C. Peters, I. Nape, A. Forbes, Tailoring light to create invariant modal spectra through complex channels. *Opt. Express* **33**, 27560–27583 (2025).
49. D. G. Pires, D. Tsvetkov, H. Barati Sedeh, N. Chandra, N. M. Litchinitser, Stability of optical knots in atmospheric *turbulence*. *Nat. Commun.* **16**, 3001 (2025).
50. I. Nape, K. Singh, A. Klug, W. Buono, C. Rosales-Guzman, A. McWilliam, S. Franke-Arnold, A. Kritzinger, P. Forbes, A. Dudley, A. Forbes, Revealing the invariance of vectorial structured light in complex media. *Nat. Photonics* **16**, 538–546 (2022).
51. C. Peters, M. Cox, A. Drozdov, A. Forbes, The invariance and distortion of vectorial light across a real-world free space link. *Appl. Phys. Lett.* **123**, 021103 (2023).
52. Y. Shen, Q. Zhang, P. Shi, D. Luping, X. Yuan, A. V. Zayats, Optical skyrmions and other topological quasiparticles of light. *Nat. Photonics* **18**, 15–25 (2024).
53. A. A. Wang, Z. Zhao, Y. Ma, Y. Cai, R. Zhang, X. Shang, Y. Zhang, J. Qin, Z.-K. Pong, T. Marozsák, B. Chen, H. He, L. Luo, M. J. Booth, S. J. Elston, S. M. Morris, C. He, Topological protection of optical skyrmions through complex media. *Light Sci. Appl.* **13**, 314 (2024).
54. C. Peters, K. Everts, T. Kleine, P. Ornelas, A. Forbes, Seeing through randomness with topological light. arXiv:2508.12305 [physics.optics] (2025).
55. L. Wang, S. Liu, G. Chen, Y. Zhang, C. Li, G. Guo, The robustness of skyrmion numbers of structured optical fields in atmospheric turbulence. *Opt. Commun.* **579**, 131568 (2025).
56. Z. Guo, C. Peters, N. Mata-Cervera, A. N. Vetlugin, R. Guo, P. Zhang, A. Forbes, Y. Shen, A. Forbes, Y. Shen, Topological robustness of classical and quantum optical skyrmions in atmospheric turbulence. arXiv:2509.05727 [physics.optics] (2025).
57. P. Ornelas, I. Nape, R. de Mello Koch, A. Forbes, Non-local skyrmions as topologically resilient quantum entangled states of light. *Nat. Photonics* **18**, 258–266 (2024).
58. P. Ornelas, I. Nape, R. de Mello Koch, A. Forbes, Topological rejection of noise by quantum *skyrmions*. *Nat. Commun.* **16**, 2934 (2025).
59. Q. Zhan, Cylindrical vector beams: From mathematical concepts to applications. *Adv. Opt. Photonics* **1**, 1–57 (2009).
60. Y. Shen, C. Rosales-Guzmán, Nonseparable states of light: From quantum to classical. *Laser Photonics Rev.* **16**, 2100533 (2022).
61. M. A. Cox, C. Rosales-Guzmán, Real-time stokes polarimetry using a polarization camera. *Appl. Optics* **62**, 7828–7836 (2023).
62. S. M. Baumann, D. M. Kalb, L. H. MacMillan, E. J. Galvez, Propagation dynamics of optical vortices due to gouy phase. *Opt. Express* **17**, 9818–9827 (2009).
63. D. McDonald, R. Bellossi, S. Gladysz, Field demonstration of turbulence-resilient self-coherent free-space optical communications. *J. Lightwave Technol.* **43**, 6146–6153 (2025).
64. C. Peters, N. Mata-Cervera, P. Ornelas, R. Warmbier, Y. Shen, A. Forbes, Extracting topological features of skyrmionic light: A tutorial. *Adv. Photonics* **8**, 023001 (2026).
65. J. Ma, J. Yang, S. Liu, B. Chen, X. Li, C. Li, J. Liu, S. Chen, Y. Yu, S. Huo, X. Zhang, Y. He, X. Zhou, H. Ye, Y. Li, S. Xu, D. Fan, J. Wang, X. Yuan, S. Zhang, Nanophotonic quantum skyrmions enabled by semiconductor cavity quantum electrodynamics. *Nat. Phys.* **21**, 1462–1468 (2025).
66. B. Ndagano, H. Defienne, A. Lyons, I. Starshynov, F. Villa, S. Tisa, D. Faccio, Imaging and certifying high-dimensional entanglement with a single-photon avalanche diode camera. *npj Quantum Inf.* **6**, 94 (2020).
67. D. L. Fried, Greenwood frequency measurements. *J. Opt. Soc. Am. A* **7**, 946–947 (1990).
68. R. de Mello Koch, B.-Q. Lu, P. Ornelas, I. Nape, A. Forbes, Quantum skyrmions in general quantum channels. *APL Quantum* **2**, 026126 (2025).
69. B. Ndagano, B. Perez-Garcia, F. S. Roux, M. McLaren, C. Rosales-Guzman, Y. Zhang, O. Mouane, R. I. Hernandez-Aranda, T. Konrad, A. Forbes, Characterizing quantum channels with non-separable states of classical light. *Nat. Phys.* **13**, 397–402 (2017).
70. C. Peters, P. Ornelas, I. Nape, A. Forbes, Spatially resolving classical and quantum entanglement with structured photons. *Phys. Rev. A* **108**, 053502 (2023).
71. D. Tse, P. Viswanath. *Fundamentals of Wireless Communication* (Cambridge Univ. Press, 2012).

72. F. S. Roux, Infinitesimal-propagation equation for decoherence of an orbital-angular-momentum-entangled biphoton state in atmospheric turbulence. *Phys. Rev. A* **83**, 053822 (2011).
73. A. McWilliam, C. M. Cisowski, Z. Ye, F. C. Speirits, J. B. Götte, S. M. Barnett, S. Franke-Arnold, Topological approach of characterizing optical skyrmions and multi-skyrmions. *Laser Photonics Rev.* **17**, 2300155 (2023).
74. R. C. Devlin, A. Ambrosio, N. A. Rubin, J. P. Balthasar Mueller, F. Capasso, Arbitrary spin-to–orbital angular momentum conversion of light. *Science* **358**, 896–901 (2017).
75. T. Li, M. Liu, C. Chen, X. Li, J. Hou, X. Yang, S. Wang, S. Zhu, Realization of spinful metaphotonic stokes skyrmions. *J. Opt.* **26**, 09LT01 (2024).
76. T. He, Y. Meng, L. Wang, H. Zhong, N. Mata-Cervera, D. Li, P. Yan, Q. Liu, Y. Shen, Q. Xiao, Optical skyrmions from metafibers with subwavelength features. *Nat. Commun.* **15**, 10141 (2024).
77. V. Hakobyan, E. Brasselet, Q-plates: From optical vortices to optical skyrmions. *Phys. Rev. Lett.* **134**, 083802 (2025).
78. G. Ruffato, M. Massari, G. Parisi, F. Romanato, Test of mode-division multiplexing and demultiplexing in free-space with diffractive transformation optics. *Opt. Express* **25**, 7859–7868 (2017).
79. C. Li, C. Liu, C. Peters, H. Yu, S. A. Maier, A. Forbes, H. Ren, Disorder-enabled synthetic metasurfaces. arXiv:2507.04696 [physics.optics] (2025).
80. H. Bezuidenhout, C. Peters, R. Kumar, A. Forbes, I. Nape, Deep diffractive optical neural networks for detecting skyrmionic topologies of light. arXiv:2512.11115 [physics.optics] (2025).
81. V. Cocotos, A. Forbes, Orbital angular momentum with topologically controlled beam sizes. *J. Opt.* **27**, 07LT01 (2025).
82. X. Zeng, J. Fang, H. Wu, J. Wang, Y. Chen, Y. Zhou, X. Yang, C. Wang, D. Wei, H. Chen, H. Gao, Y. Shen, Tailoring ultra-high-order optical skyrmions. *Laser Photonics Rev.* **19**, e00732 (2025).
83. V. Arrizón, U. Ruiz, R. Carrada, L. A. González, Pixelated phase computer holograms for the accurate encoding of scalar complex fields. *J. Opt. Soc. Am. A* **24**, 3500–3507 (2007).
84. M. Chen, F. S. Roux, J. C. Olivier, Detection of phase singularities with a shack–hartmann wavefront sensor. *J. Opt. Soc. Am. A* **24**, 1994–2002 (2007).
85. A. A. Wang, Y. Ma, Y. Zhang, Z. Zhao, Y. Cai, X. Qiu, B. Dong, C. He, Perturbation-resilient integer arithmetic using optical skyrmions. *Nat. Photonics* **19**, 1367–1375 (2025).
86. C. He, B. Chen, Z. Song, Z. Zhao, Y. Ma, H. He, L. Luo, T. Marozsak, A. A. Wang, R. Xu, P. Huang, J. Li, X. Qiu, Y. Zhang, B. Sun, J. Cui, Y. Cai, Y. Zhang, A. Wang, M. Wang, P. Salter, J. A. J. Fells, B. Dai, S. Liu, A. Forbes, A reconfigurable arbitrary retarder array as complex structured matter. *Nat. Commun.* **16**, 4902 (2025).
87. M. A. Cox, N. Mphuthi, I. Nape, N. Mashaba, L. Cheng, A. Forbes, Structured light in turbulence. *IEEE J. Sel. Top. Quantum Electron.* **27**, 7500521 (2021).

Acknowledgments: C.P. would like to thank P. Ornelas for useful discussions regarding this project and assisting with code used in the data analysis. **Funding:** A.F. and M.C. would like to acknowledge support from the South African National Research Foundation/CSIR Rental Pool Programme. A.F. also acknowledges funding from the South African Quantum Technology Initiative. E.B. would like to acknowledge the support of IdEx University of Bordeaux and its Grand Research Program GPR LIGHT. **Author contributions:** C.P.: Writing—original draft, conceptualization, investigation, writing—reviewing and editing, methodology, resources, data curation, validation, formal analysis, software, and visualization. V.H.: Investigation, writing—reviewing and editing, data curation, and validation. A.D.: Investigation, writing—original draft, and methodology. E.B.: Writing—reviewing and editing, funding acquisition, and supervision. M.C.: Conceptualization, methodology, resources, writing—reviewing and editing, supervision, and funding acquisition. A.F.: Writing—original draft, conceptualization, investigation, writing—reviewing and editing, methodology, resources, funding acquisition, data curation, validation, supervision, formal analysis, project administration, and visualization. **Competing interests:** The authors declare that they have no competing interests. **Data, code, and materials availability:** All data and code needed to evaluate and reproduce the results in the paper are present in the paper and/or the Supplementary Materials. Measured data are stored on Zenodo and can be accessed via https://zenodo.org/records/20025323 (DOI: 10.5281/zenodo.20025323). This study did not generate new materials.

Submitted 28 November 2025
Accepted 7 July 2026
Published 14 August 2026
10.1126/sciadv.aee2671

Science Advances

Topological robustness of optical skyrmions through a real-world free-space link

Cade Peters, Vagharshak Hakobyan, Alice Drozdov, Etienne Brasselet, Mitchell Cox, and Andrew Forbes

Sci. Adv. **12** (33), eaee2671. DOI: 10.1126/sciadv.aee2671

Science Advances (ISSN 2375-2548) is published by the American Association for the Advancement of Science. 1200 New York Avenue NW, Washington, DC 20005. The title *Science Advances* is a registered trademark of AAAS.